ADAPTIVE MODEL FOLLOWING CONTROL METHOD FOR ACTIVELY CONTROLLED MAGNETIC BEARING MOMENTUM WHEEL

Y.-C. Xie
C.O.E. research fellow of Institute of Space and Astronautical Science (ISAS) on leaving from Beijing Institute of Control Engineering, P. R. China

H. Sawada, T. Hashimoto, and K. Ninomiya
Institute of space and Astronautical Science, 3-1-1 Yoshinodai, Sagamihara, 229-8510, Japan

ABSTRACT

For the active control of magnetic bearing momentum wheels that could be used as actuators of high-accuracy spacecraft attitude control system, an adaptive model following control method is presented in this paper. This method is featured by adaptive bandwidth-regulation mechanism, controller with logical derivative, new nutation damping network, and non-linearity compensator. Thus it is convenient to make compromise between fast dynamic response and active-vibration suppression at harmonic frequencies of the wheel rotation. The robust stability of this method is analyzed and digital simulation is carried out. Simulation results show that this method has great capability of active-vibration suppression, good dynamic response, and satisfactory nutation damping of the wheel rotor for a large range of wheel rotational speed.

INTRODUCTION

For the high-accuracy attitude control of spacecraft, Magnetic Bearing Momentum Wheel (MBMW) is being investigated as an actuator because of its merits of low disturbance characteristics [1, 2] and gimballability when a suitable active controller is used. In this context, the active control of MBMW means to make the rotor spin around its principal axis of inertia to achieve low disturbance input while being able to tilt the principal axis of inertia for attitude control of spacecraft. This has to be done with adequate nutation damping of the wheel rotor. The performance requirements for the active control system of MBMW are usually as follows:

(1) Good active-vibration suppression of inevitable sensor errors. Since the band-limited white noise is easy to be suppressed by using a low pass filter, the components to be suppressed by means of active-

vibration suppression are mainly those disturbance components with harmonic frequencies of the wheel rotation. In [2] Active-Vibration Suppression (AVS) is defined, which means to enable the rotor to rotate about its principle axis of inertia and suppress all the resulting noise components from the whirling and wobbling sensor surface without affecting suspension stability. This term is adopted through this paper.

(2) Robustness against electromagnetic non-linearity.

(3) Good disturbance suppression against wheel external environmental disturbance torques.

(4) Robustness against wheel rotational speed in a large range.

In previous literature, considering the non-linearity of electromagnets, Nam et al. [1] applied the H_∞ robust control method to the active control of MBMW, but only a fixed rotational speed is considered. Without thinking of the non-linearity of electromagnets, Bichler [2] proposed a Model Following Control (MFC) method and indicated that this method has superior capability of active-vibration suppression for a large range of wheel rotational speed. However, this method is based on a special observer to realize active-vibration suppression, thus its response to fast externally impressed torques and movements is slow. If external environmental disturbance torques which have been mentioned already exist, large overshoot and small nutation of the wheel rotor will be excited when wheel rotational speed is low. Therefore, in order to solve the above problems and to realize the active control of MBMW with non-linear electromagnets, an Adaptive Model Following Control (AMFC) method is proposed in this paper.

In this new method, first an adaptive mechanism is inserted into the above model following control method. This adaptive mechanism can adaptively regulate the bandwidth of a special observer based on on-line characteristic identification so as to improve system dynamic response if needed. Second, logical derivative [3] is applied to the controller design to reduce overshoot further. Third, a new nutation damping method that can automatically adjust the gain of nutation damping according to wheel speed is introduced in order to obtain consistent nutation damping rate for different wheel speed. Finally, a non-linearity compensator is put forward to overcome electromagnetic non-linearity. Consequently, the adaptive model following control method is suitable for the active control of MBMW.

In this paper, the mathematical model of MBMW is introduced first. Then the adaptive model following control method is presented. Since the closed-loop system is a nonlinear and time-varying system, the robust stability of this method is analyzed from the engineering viewpoint. To verify the effectiveness of this new method, digital simulation is carried out and the possible application of this method to the active control of MBMW for spacecraft attitude control is discussed at the end.

MBMW

Although the control method presented in this paper could be applied to any actively controlled MBMW, the authors select a specific type of MBMW and apply the method to the control of this kind of wheel.

Octa-Electromagnet-Type Active Magnetic Bearing Momentum Wheel

For future three-axis spacecraft attitude control, Octa-Electromagnet-Type Active Magnetic Bearing Momentum Wheel (OETA-MBMW), which is a kind of five-degree of freedom MBMW, is developed in ISAS [1, 4]. OETA-MBMW is composed of eight electromagnets whose attractive forces have components both in axial and in radial direction so that it may serve to reduce size and weight. Eight gap sensors are symmetrically installed with tilts so as to measure the rotor displacements in three directions and gimballing angles around two axes vertical to the wheel rotational axis. The cross section of this kind of OETA-MBMW is shown in Fig. 1.

Wheel Dynamics

In describing the rotational motion of the MBMW, rotational coordinate systems are used as shown in Fig. 2, in which coordinate system $X_0Y_0Z_0$ is considered as spacecraft's attitude reference coordinate system while $X_wY_wZ_w$ a wheel-body coordinate. $X_0Y_0Z_0$ changes so slowly in inertial space that it can be considered as an inertial coordinate system for the present purpose. Angles ϕ_w, θ_w and φ_w are the Euler angles in X-Z-Y transformation from $X_0Y_0Z_0$ to $X_wY_wZ_w$. For the simplicity of motion derivation, spin-free coordinate system $X_{2w}Y_{2w}Z_{2w}$ is used to describe the dynamic motion of MBMW [1].

Suppose that the selected coordinates are on the principal axes, the gimballing angles of MBMW are small, the wheel is rigid and symmetric about its rotational axis, and the wheel rotational speed varies so slowly with time that it can be considered as constant [1]. Then the linearized dynamic model of MBMW in gimballing axes can be expressed as follows.

$$\begin{cases} \ddot{\phi}_w - \sigma\Omega\dot{\varphi}_w = (T_x + T_{dx})/J_w \\ \ddot{\varphi}_w + \sigma\Omega\dot{\phi}_w = (T_z + T_{dz})/J_w \end{cases} \tag{1}$$

In (1), $\sigma = J_{yw}/J_w$ is the ratio of moments of inertia. J_{wx}, J_{wy} and J_{wz} are inertial moments of the wheel in X_w, Y_w and Z_w axis, respectively, and $J_{wx} = J_{wz} = J_w$ can safely be assumed. $\Omega = \dot{\theta}_w$ is wheel rotational speed. T_x and T_z are electromagnetic torques. T_{dx} and T_{dz} are external environmental disturbance torques including those due to eddy current loss, ohmic loss and those exerted from the spacecraft body on which the physical space-environmental torque acts.

According to experimental data, the model of electromagnet can be modeled as accurately as follows [4].

$$\begin{cases} T_x = k_m \phi_g^2 \left(\dfrac{V_b + v_\phi}{\phi_g - \phi} \right)^2 - k_m \phi_g^2 \left(\dfrac{V_b - v_\phi}{\phi_g + \phi} \right)^2 \\ T_z = k_m \varphi_g^2 \left(\dfrac{V_b + v_\varphi}{\varphi_g - \varphi} \right)^2 - k_m \varphi_g^2 \left(\dfrac{V_b - v_\varphi}{\varphi_g + \varphi} \right)^2 \end{cases} \quad (2)$$

In (2), k_m is electromagnetic gain, ϕ_g and φ_g are nominal electromagnetic gaps, ϕ and φ are electromagnetic gaps, and satisfy $|\phi| < \phi_g$, $|\varphi| < \varphi_g$. If we neglect the attitude motion of spacecraft, then $\phi = \phi_w$ and $\varphi = \varphi_w$. V_b is a constant representing bias voltage applied to electromagnets, v_ϕ and v_φ are control commands or control voltages, and satisfy $|v_\phi| < V_b$, $|v_\varphi| < V_b$.

According to (2) we know that the non-linearity of electromagnets is proportional and inversely proportional in the second order for voltage-input and the gimballing angles of the wheel, respectively. Although, in order to overcome this kind of electromagnetic non-linearity, a constant pre-magnetization bias voltage V_b is added, the electromagnetic torque-output is still not pure linear function of control voltage-input. By using Taylor expansion, the first-order approximation of (2) can be expressed in (3).

$$\begin{cases} T_x = k_{EM} v_\phi + k_{N\phi} \phi \\ T_z = k_{EM} v_\varphi + k_{N\varphi} \varphi \end{cases} \quad (3)$$

Where $k_{EM} = 4k_m V_b$, $k_{N\phi} = 4k_m V_b^2 / \phi_g$, $k_{N\varphi} = 4k_m V_b^2 / \varphi_g$.

Gap Sensors

Following sensor noises of MBMW are considered in gap sensor model according to wheel mechanism [4].

(1) Sensor noise resulting from the electric noise components of gap sensors is modeled as white noise $(\zeta_\phi, \zeta_\varphi)$ whose frequency band is limited to the controller's sampling frequency.

(2) Harmonic sensor noises caused by imbalance of rotor, i.e. the geometric axis of rotor is not coincident with the principal axis of inertia, and mechanical imperfections of the rotating part are modeled with the harmonic signals of wheel rotational speed shown as follows.

$$\begin{cases} n_\phi = \sum_{i=1}^{N_c} c_i \sin(i * \theta_w + \theta_i) \\ n_\varphi = \sum_{i=1}^{N_c} c_i \sin(i * \theta_w + \theta_i + \pi/2) \end{cases} \quad (4)$$

In (4), N_s is the number of harmonics, c_i is the amplitude of harmonics, and θ_i is initial angle. As a result, the model of gap sensors can be expressed in (5).

$$\begin{cases} \tilde{\phi}_w = \phi_w + \sum_{i=1}^{N_s} c_i \sin(i*\theta_w + \theta_i) + \zeta_\phi \\ \tilde{\varphi}_w = \varphi_w + \sum_{i=1}^{N_s} c_i \sin(i*\theta_w + \theta_i + \pi/2) + \zeta_\varphi \end{cases} \tag{5}$$

ADAPTIVE MODEL FOLLOWING CONTROL METHOD

AMFC method is proposed based on MFC method [2], thus it keeps the basic structure of MFC method and inherits MFC's advantages. However, AMFC method is superior to MFC method because of its adaptive mechanism for AVS, controller with logical derivative, new nutation damping strategy and non-linearity compensator.

The block diagram of the AMFC closed-loop system for the active control of the rotor-tilt-loops of MBMW is shown in Fig. 3. In Fig. 3, the right part enclosed by dash-line frame represents the plant to be controlled, i.e. MBMW, while the other left part represents AMFC's control loop.

The block of AMF-AVS in Fig. 3 is demonstrated in Fig. 4. In Figure 4, *integrator I* and *integrator II* are standard integrators. *Low pass filter* is a first-order low pass filter that can be represented as $\frac{a}{s+a}$, where a is positive real number. k_{11}, k_{12}, k_{21} and k_{22} are observer coefficients, *Gain* represents the gain coefficient of the plant to be controlled from electromagnet input to rotor output. For the plant discussed in this paper, *Gain* equals to k_{EM0}/J_{w0}, where k_{EM0} and J_{w0} represent the nominal values of k_{EM} and J_w, respectively. In the following parts of this paper, the variable with subscript 0 also denotes the nominal value of this variable. *Adaptive mechanism* automatically determines when k_{21} and k_{22} should be switched on or switched off so that the bandwidth of AMF-AVS observer is regulated adaptively. In fact, the AMF-AVS loop in Fig. 4 can be considered as a special adaptive observer of rotor movements.

In Fig. 3, *gyro-decoupling* network uses the same decoupling network proposed in [5], which is depicted in (6).

$$\begin{cases} u_{gx} = -\sigma_0 \Omega_0 \frac{1}{s} u_z \\ u_{gz} = \sigma_0 \Omega_0 \frac{1}{s} u_x \end{cases} \tag{6}$$

Where, u_x and u_z are the inputs of the *gyro-decoupling* network while u_{gx} and u_{gz} the outputs.

In Fig. 3, *Controller* can be designed as single-input and single-output controller because of the effect of *gyro-decoupling* network. *Nutation damping* network is used to damp down the nutation

deteriorated by AMF-AVS and wheel external environmental disturbance torques. *Non-linearity compensator* is employed to compensate electromagnetic non-linearity.

In the following sections, adaptive mechanism of AMF-AVS, controller with logical derivative, new nutation damping strategy and non-linearity compensator will be explained in detail.

Adaptive Mechanism of AMF-AVS

In [2], to control the faster externally impressed stator movements, a *limit switch* is used to quicken the convergence of AVS observer by detecting the difference of the rotor real position and the observer output. If the difference exceeds half of the nominal gap, a second stronger feedback is turned on to force the observer output immediately to the real position to prevent a touch down of the rotor. The block diagram of AVS of MFC method is shown in Fig. 5. In fact, this kind of limit switch can not control the faster externally impressed stator movements. The reason is that the limit switch works only after the difference exceeds half of the nominal gap, and even in this case stronger feedback in observer tends to result in larger controller output than the input voltage limit of the electromagnets, which means this effort is in vain. **Furthermore, even if the second stronger feedback works, the low noise quality of AVS is reduced** because unfiltered sensor signal is introduced directly into the control system. In order to solve this problem and to make a good compromise between fast convergence of observer and satisfactory active-vibration suppression in the whole gap range, adaptive bandwidth-regulation method is proposed to replace the limit switch of MFC for AVS.

The main idea of the adaptive bandwidth-regulation method is to broaden the observer bandwidth when fast convergence is needed, for example when large overshoot occurs in gimballing angles, and to reduce the observer bandwidth when active-vibration suppression is the main purpose, for example at the steady state. Moreover, in this method the saturation non-linearity of the input voltage of electromagnets is also considered. The adaptive bandwidth-regulation is based on on-line characteristic identification.

As defined in Fig. 4, y_lpf is the output of AMF-AVS low-pass filter. Define the average value of y_lpf in one wheel rotational period as y_ave. y_ave is refreshed every one wheel rotational period. The rule for determining when k_{21} and k_{22} should be turned on/off is depicted as follows.

Rule 3.1.

If $|y\_ave| > \delta_1$ and $|y\_ave| < \delta_2$,
then k_{21} and k_{22} are switched on,
else k_{21} and k_{22} are switched off.

In Rule 3.1, δ_1 is named as steady-state threshold, and is determined according to the index of steady state and the amplitude of sensor noises. δ_2 is named as saturation threshold, and is determined according to the input voltage limit of electromagnets and controller.

Rule 3.1 means that if the average difference of the observer output and the rotor position is much

larger than the sensor noises and smaller than the saturation threshold, which can make sure the controller output is less than the input voltage limit, the bandwidth of AMF-AVS observer is broadened. This kind of bandwidth regulation can make the observer output follow the rotor position quickly and effectively. Therefore the adaptive bandwidth-regulation method can improve system dynamic response while active-vibration suppression is guaranteed.

Controller with Logical Derivative

Logical derivative was proposed in [3] to improve system dynamic response, especially to reduce system overshoot. The controller with logical derivative is designed in such a way. First design a Proportional- Integral-Derivative (PID) controller, then modify the derivative coefficient according to a certain logical rule.

After introducing logical derivative the controller for single-axis gimballing control is designed as follows.

$$u = k_p e + k_i \int e dt + k_d' \dot{e} . \tag{7}$$

In (7), u is controller output, e is the difference between position command and AMF-AVS observer output,

$$\begin{cases} k_d' = k_d & if\ (e\dot{e} \le 0\ or\ in\ steady\ state) \\ k_d' = k_{logic} k_d & else \end{cases}$$

k_p, k_i and k_d are PID coefficients, k_d' is logical derivative coefficient, k_{logic} is the modifying coefficient for logical derivative and $k_{logic} \ge 1$. As discussed above, If $|e| < \delta_3$ is satisfied continuously for more than N_s sampling periods then we say that system is '*in steady state*'. Where δ_3 is the required steady state error and N_s is positive integer.

In the transient process, suitable k_{logic} leads to high controller bandwidth and phase lead, thus logical derivative can improve system dynamic response. However, in the steady state, the controller with logical derivative becomes a standard PID controller, hence logical derivative doesn't affect the stability of the whole control system [3].

Nutation Damping

In this paper, a new nutation damping strategy is proposed to damp down the nutation deteriorated by AMF-AVS and wheel external environmental disturbance torques. The nutation damping cross coupling network for tilt loops is shown as follows.

$$\begin{cases} u_{nx} = -\dfrac{k_{nut}}{k_{EM0}} J_{wy0}\Omega_0 \dfrac{\kappa s^2}{s^2 + \kappa s + (\sigma_0\Omega_0)^2} \cdot \dfrac{b}{s+b}\tilde{\varphi}_w \\ u_{ny} = -\dfrac{k_{nut}}{k_{EM0}} J_{wy0}\Omega_0 \dfrac{\kappa s^2}{s^2 + \kappa s + (\sigma_0\Omega_0)^2} \cdot \dfrac{b}{s+b}\tilde{\phi}_w \end{cases} \tag{8}$$

In (8) $\dfrac{\kappa s^2}{s^2 + \kappa s + (\sigma_0\Omega_0)^2}$ is a bandwidth filter, and κ is a positive real number. $\dfrac{b}{s+b}$ is a low pass filter, and b is a positive real number. k_{nut} is nutation damping gain and $k_{nut} > 0$.

The advantage of this nutation damping method is that the declining rate of nutation damping is independent of wheel rotational speed because the parameters of the nutation-damping network are functions of wheel rotational speed. In addition, by choosing a suitable nutation-damping gain, this nutation damping method is easy to realize nutation damping for MBMW with large time delay.

Non-linearity Compensator

According to (3), a compensator for making up for electromagnetic non-linearity in the tilt loops is designed as follows.

$$\begin{cases} u_{cx} = -\dfrac{k_{N0}}{k_{EM0}}\phi_e \\ u_{cy} = -\dfrac{k_{N0}}{k_{EM0}}\varphi_e \end{cases} \tag{9}$$

In (9), u_{cx} and u_{cy} are the non-linearity compensator outputs while ϕ_e and φ_e are the non-linearity compensator inputs or the observer outputs.

ROBUST STABILITY

According to the above two sections, we know that the closed-loop system containing the plant to be controlled, i.e. MBMW itself, and AMFC's control loop is nonlinear and time varying. Therefore, the following robust stability analysis follows an engineering method.

The AMFC only has its observer adaptively switched between two groups of parameters. One group of parameters is $[k_{11}\ k_{12}\ k_{21\_off}\ k_{22\_off}] \triangleq \boldsymbol{K}_1$, the other group of parameters is $[k_{11}\ k_{12}\ k_{21\_on}\ k_{22\_on}] \triangleq \boldsymbol{K}_2$. If characteristic variable $|y\_ave|$ is larger than a steady-state threshold δ_1 and smaller than a saturation

threshold δ_2, then K_2 is switched on as observer parameters, otherwise K_1 is switched on. Since y_ave is the average value of y_lpf in one wheel rotational period, then y_lpf can be expressed as $y\_lpf \approx y\_ave + f(\Omega, 2\Omega, \cdots)$, where $\Omega = 2\pi/T_w$ and T_w is wheel rotational period. Suppose that both the closed-loop system containing K_1 and the closed-loop system containing K_2 are exponentially stable. Define area $I = \{y\_ave \mid |y\_ave| \le \delta_1\}$, area $II = \{y\_ave \mid \delta_1 < |y\_ave| < \delta_2\}$, and area $III = \{y\_ave \mid |y\_ave| \ge \delta_2\}$. Since $\delta_1 << \delta_2$, then the stability analysis in area I, II and III can be carried on equivalently and separately in area I and II, and area II and III. First consider the stability in area I and II. If at time $N_1 T_w$ (N_1 is an integer), $|y\_ave| > \delta_1$ and K_2 is switched on, then an integer N_2 ($N_2 > N_1$) must exist so that at time $N_2 T_w$, $|y\_ave| \le \delta_1$ and the observer parameters are switched to K_1. From time $N_2 T_w$, if $|y\_ave|$ keeps smaller than δ_1, then it will converge to zero and the amplitude of $f(\Omega, 2\Omega\cdots)$ will converge too. After time $N_2 T_w$, if $|y\_ave|$ is larger than δ_1 again, then it must become smaller at another time $N_3 T_w$ ($N_3 > N_2$, N_3 is an integer). If K_1 and K_2 are designed suitably, then after several times switches, the closed-loop system will converge to steady state. By the same kind of discussion, the stability in area II and III can also be analyzed if the saturation non-linearity does not make system unstable. As a result, If K_1, K_2, δ_1, δ_2 and controller are designed reasonably, after finite times of switches the closed-loop system will enter steady state. In simulation, only one to three times switches occurred.

According to the transfer function of the closed-loop system, the exponential stability and robustness of the closed-loop system including K_1 and the closed-loop system including K_2 are analyzed separately. For the MBMW whose parameters are listed in Table 1, and the AMFC's control loop whose parameters are as listed in Table 2, the robust stability range of J_w, k_{EM}, $k_{N\phi}$, $k_{N\varphi}$, Ω, and σ as a whole, i.e. $[J_w/J_{w0} \;\; k_{EM}/k_{EM0} \;\; k_{N\phi}/k_{N\phi 0} \;\; k_{N\varphi}/k_{N\varphi 0} \;\; \Omega/\Omega_0 \;\; \sigma/\sigma_0] = \Sigma/\Sigma_0\,[1 \;\; 1 \;\; 1 \;\; 1 \;\; 1 \;\; 1]$, is demonstrated in Table 3. Considering the time delay in electromagnets, which is modeled as $\frac{1}{\tau s + 1}$, where τ is time constant and $\tau = 0.01\,\text{sec}$, the robust stability range of J_w, k_{EM}, $k_{N\phi}$, $k_{N\varphi}$, Ω, and σ as a whole is demonstrated in Table 4.

For case H in Table 3, the root loci of the closed-loop system with respect to Σ/Σ_0 is demonstrated in Fig. 6, respectively. In Fig. 6, asterisks show the positions of the poles of the closed-loop system when J_w, k_{EM}, $k_{N\phi}$, $k_{N\varphi}$, Ω, and σ reach their nominal values, i.e. $\Sigma/\Sigma_0 = 1$.

Table 1 parameters of MBMW

J_w	σ	k_{EM}	$k_{N\phi}(k_{N\varphi})$	V_b	N_s	ϕ_g	φ_g	c_1, c_3, c_5	c_2, c_4, c_6
0.0129 kgm^2	1.85	0.0448Nm/V	3.4225Nm	0.8V	6	0.6deg	0.6deg	0.004deg	0.0005deg

Table 2 parameters of AMFC's control loop

κ	b	k_p gain	k_i gain	k_d gain	k_{11}	k_{12}	k_{21}	k_{22}	a	k_{mul}	k_{log}	δ_1	δ_2
32	10	121.2	150	15.64	1	2	0/20	0/5	25	k_{EM0}	5	10^{-5}	0.0035

Table 3 robust stability range of AMFC when τ =0 sec

Case	k_{11}	k_{12}	k_{21}	k_{22}	σ	r (rpm)	Σ/Σ_0
A	1	2	20	5	1.6	1000	0.7 ~ 1.24
B	↓	↓	↓	↓	↓	6000	0.6 ~ 1.25
C	↓	↓	↓	↓	1.85	1000	0.7 ~ 1.24
D	↓	↓	↓	↓	↓	6000	0.6 ~ 1.25
E	↓	↓	0	0	1.6	1000	0.6 ~ 1.47
F	↓	↓	↓	↓	↓	6000	0.4 ~ 1.47
G	↓	↓	↓	↓	1.85	1000	0.5 ~ 1.47
H	↓	↓	↓	↓	↓	6000	0.4 ~ 1.47

Table 4 robust stability range of AMFC when τ =0.01 sec

Case	A	B	C	D	E	F	G	H
Σ/Σ_0	0.7 ~ 1.03	0.6 ~ 1.0	0.7 ~ 1.02	0.6 ~ 1.0	0.6 ~ 1.03	0.4 ~ 1.0	0.6 ~ 1.02	0.4 ~ 1.0

SIMULATION

The AMFC method, MFC method [2], and H_∞ control method [1] are simulated for comparison. Both AMFC and MFC use the same kind of non-linearity compensator proposed in this paper. The parameters of MBMW are listed in Table 1. The parameters of AMFC's control loop are as listed in Table 2. MFC has the same parameters as AMFC except for adaptive mechanism, logical derivative, and nutation damping. The H_∞ controller is an eighth-order controller. The characteristics of electromagnetic non-linearity are shown in Fig. 7. In simulation, a step external environmental disturbance whose amplitude is 0.0005Nm is inserted in φ_w channel. The simulation results are shown in Fig. 8(a, b)~ Fig. 12(a, b).

Fig. 8(a, b) ~ Fig. 11(a, b) show the true values of the gimballing angles when MFC/AMFC control method is used and when the wheel rotational speed is 1000rpm and 6000rpm, respectively. Fig. 12(a, b) show the true values of the gimballing angles when H_∞ / AMFC control method is used and when the wheel rotational speed is 4000rpm.

Simulation results show that both AMFC method and MFC method are robust against wheel

rotational speed in a large range and have much better active-vibration suppression compared with H_∞ control method, although by using H_∞ control method almost no overshoot occurs. However, compared with MFC method, AMFC method keeps much smaller overshoot and shorter settling time for different wheel rotational speed and different position commands. Simulation results also show that the new nutation damping method is very effective for a large range of wheel rotational speed.

Although in simulation the AMFC method is only applied to a specific MBMW, the AMFC method is easy to be applied to any kind of actively controlled MBMWs. Furthermore, the AMFC method is also easy to realize in practical engineering. Applying the AMFC method to a prototype actively controlled MBMW owned by ISAS is being considered.

CONCLUSION

In this paper adaptive model following control method is presented. This method relies on adaptive bandwidth-regulation mechanism, controller with logical derivative, new nutation damping network and non-linearity compensator. Consequently this method is convenient to make compromise between dynamic response and active-vibration suppression at harmonic frequencies of the wheel rotation, and to damp nutation of the wheel rotor while keeping the closed-loop system stable.

Study results show that this method has great capability of active-vibration suppression, good dynamic response, and satisfactory nutation damping for a large range of wheel rotational speed. The robustness of this method with respect to system uncertain parameters is also strong. Therefore it is easy and possible to realize high-accuracy spacecraft attitude control by using the MBMW controlled by the AMFC method. Now, applying the MBMW controlled by the AMFC method to spacecraft attitude control is being considered.

ACKNOWLEDGEMENTS

The authors would like to express their honest thanks to Prof. I. Nakatani, Prof. T. Kubota (both of ISAS) and Dr. M. Inoue of Mitsubishi Electric Corporation for their useful comments.

REFERENCES

[1] M.-R. Nam, T. Hashimoto and K. Ninomiya. Design of H_∞ Attitude Controllers for Spacecraft Using

a Magnetically Suspended Momentum Wheel. European Journal of Control (1997), 3:114-124.

[2] U. J. Bichler. A Low Noise Magnetic Bearing Wheel for Space Application. 2nd International Symposium on Magnetic Bearing, July 12-14, 1990, Tokyo, Japan, 1-8.

[3] Yong-Chun Xie, Hong-Xin Wu, Zhen-Duo Lu. The All-Coefficient Adaptive Control Method and Its Application in Spacecraft Attitude Control. Space Technology, Vol.16, No.5/6, pp.331-336, 1996.

[4] Myeong-Ryong Nam, Studies on the Attitude Control System for Spacecraft Employing a Magnetically-Suspended Momentum Wheel, Doctoral Dissertation, University of Tokyo, 1997.

[5] U. Bichler, T. Eckardt, A 3(5) Degree of Freedom Electro-dynamic Bearing Wheel for 3-axis Spacecraft Attitude Control Applications, proceedings of the First International Symposium on Magnetic Bearings, ETH Zurich, June 6-8, 1988.

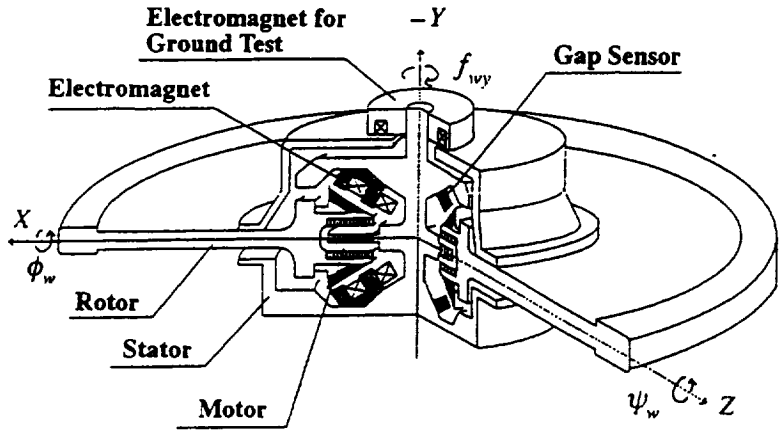

Fig. 1 Cross section of Octa-Electromagnet-Type Active Magnetic Bearing Momentum Wheel

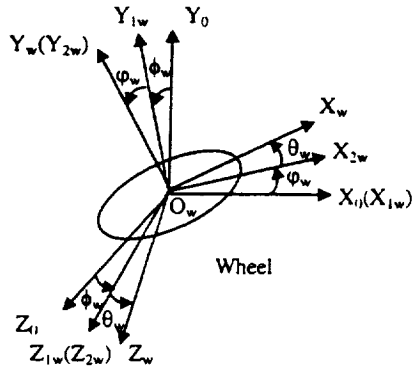

Fig. 2 Coordinate systems of MBMW

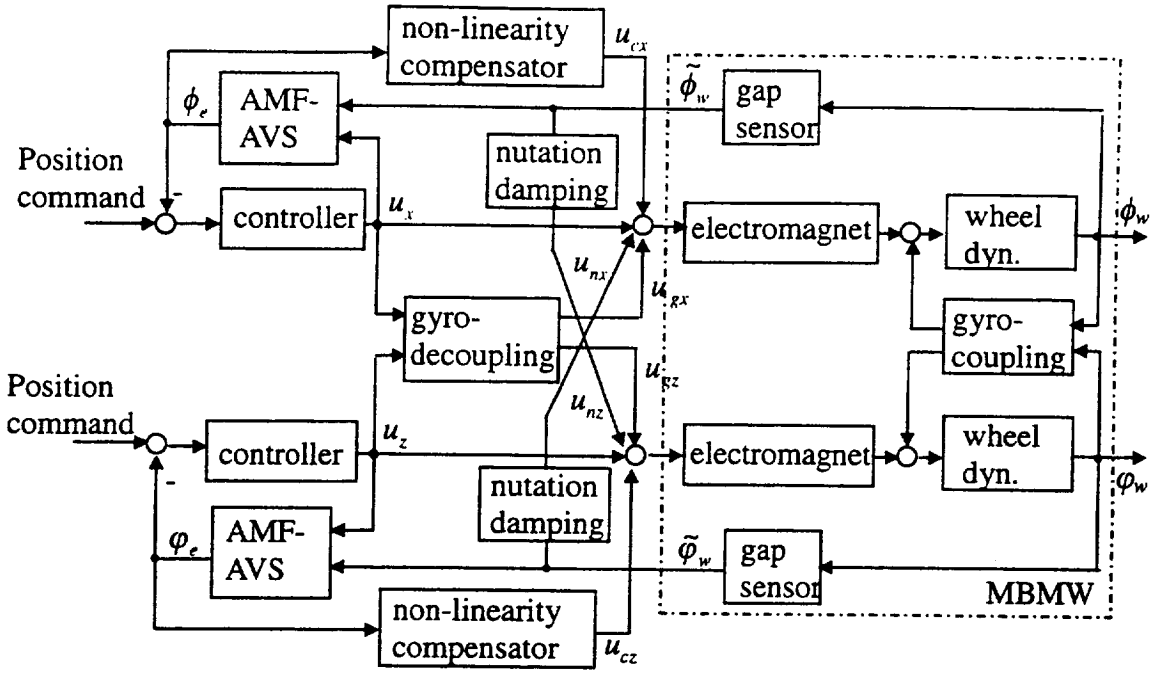

Fig. 3 AMFC in the tilt loops of MBMW

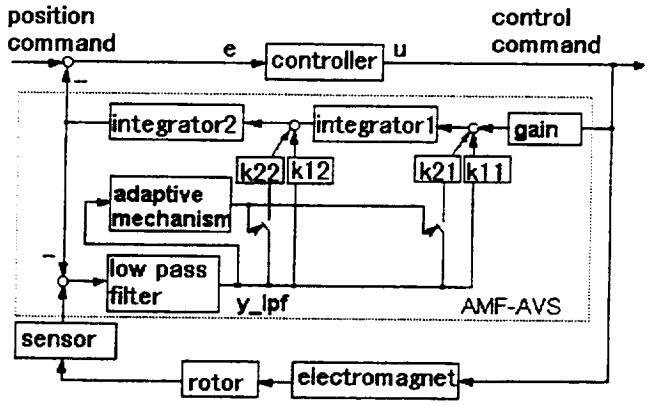

Fig. 4 Block diagram of AMF- AVS of AMFC

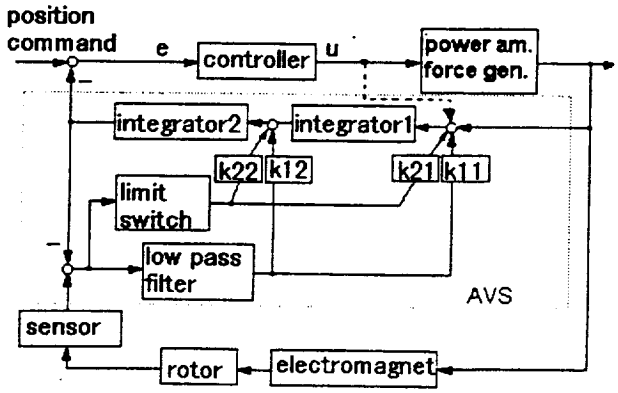

Fig. 5 Block diagram of AVS of MFC

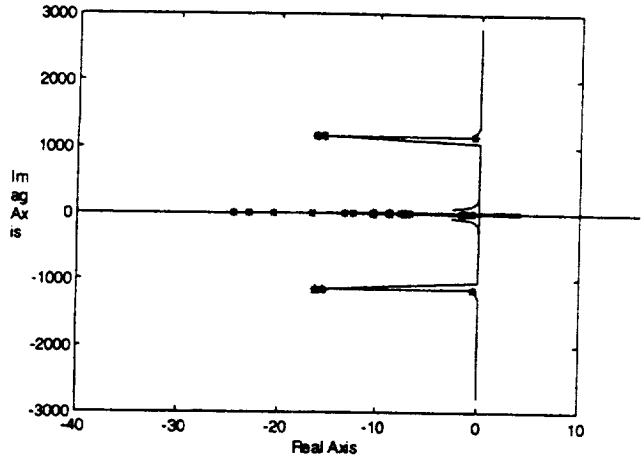

Fig. 6 Root locus of the closed-loop system with respect to Σ/Σ_0
(case H, $\Sigma/\Sigma_0 \in [0.25, 1.55]$)
(critical points: $\Sigma/\Sigma_0 = 0.34, 1.47$)

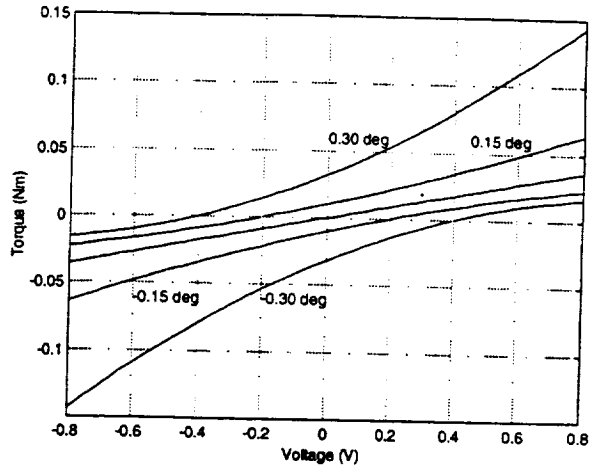

Fig. 7 Characteristics of electromagnetic non-linearity

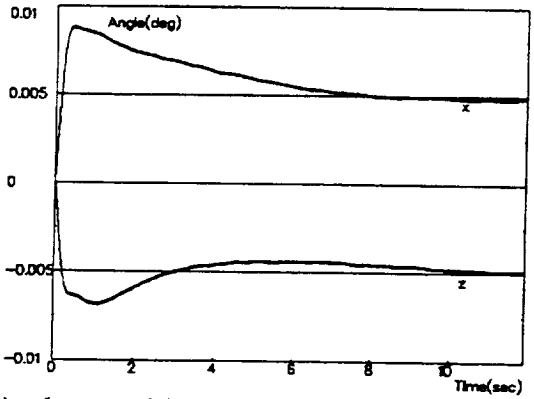

(a) when position commands are ± 0.005deg

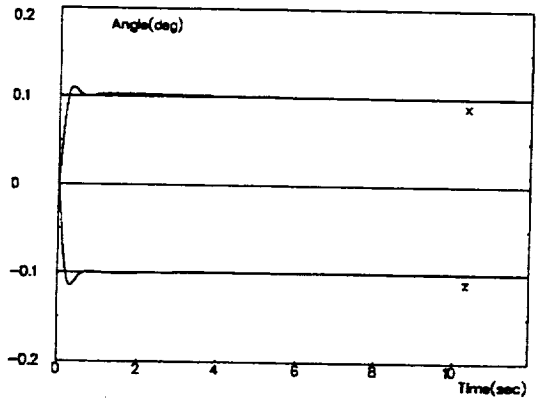

(b) when position commands are ± 0.1deg

Fig. 8 Simulation results of MFC method (1000rpm)

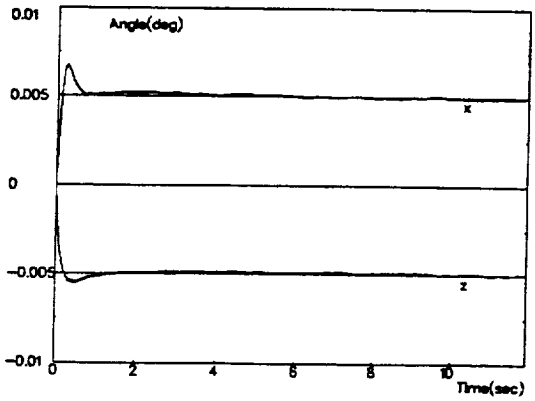

(a) when position commands are ± 0.005deg

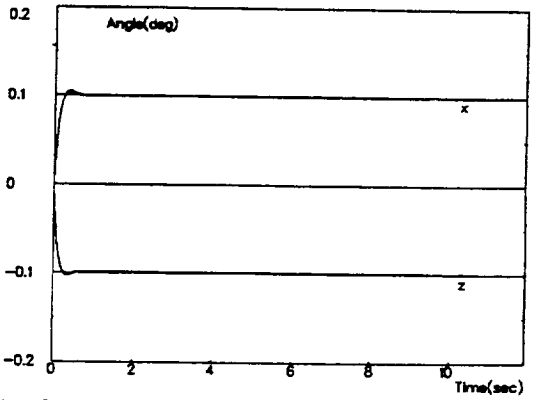

(b) when position commands are ± 0.1deg

Fig. 9 Simulation results of AMFC method (1000rpm)

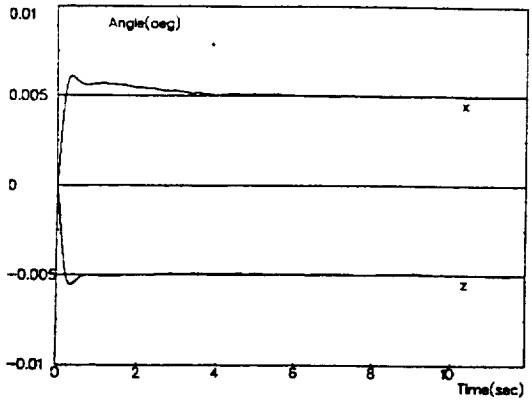

(a) when position commands are ± 0.005deg

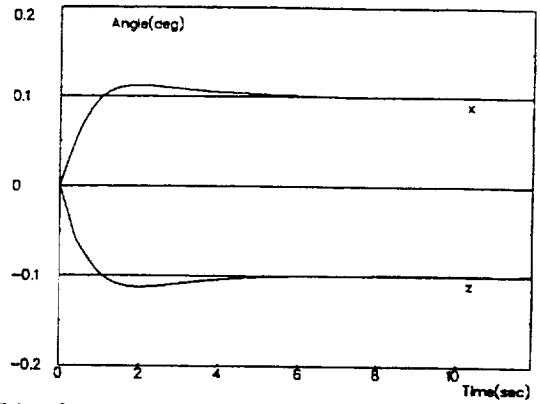

(b) when position commands are ± 0.1deg

Fig. 10 Simulation results of MFC method (6000rpm)

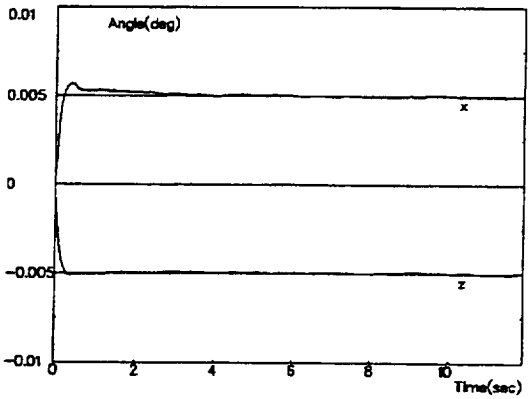

(a) when position commands are ± 0.005deg

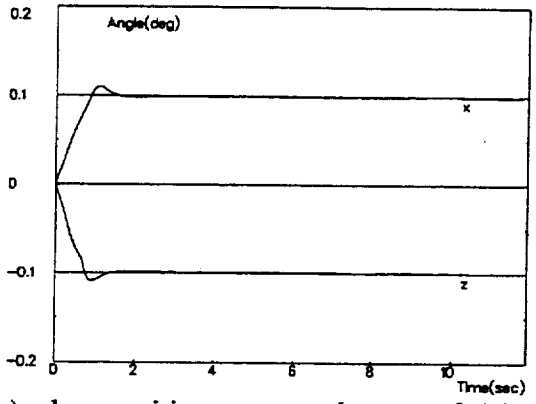

(b) when position commands are ± 0.1deg

Fig. 11 Simulation results of AMFC method (6000rpm)

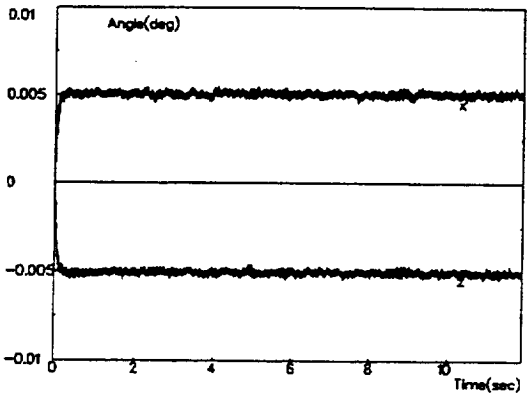

(a) H_∞ control method

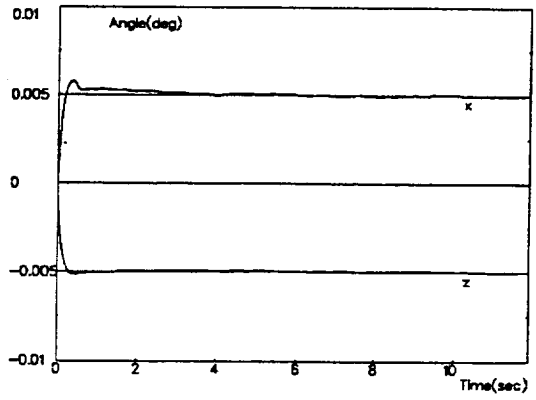

(b) AMFC method

Fig. 12 Simulation results (4000rpm)